الجمهورية الجزائرية الديمقراطية الشعبية

وزارة التعليم العالي والبحث العلمي

YAHIA FARES – MEDEA UNIVERSITY

جامعة يحي فارس – المدية

Faculty: Technology

Department: Mechanical Engineering

Specialty: Materials and Surface Engineering

Thesis

Presented in partial fulfillment of the requirements for the degree of the Master 2 Diploma

Theme

Influence of Al addition on the microstructure, and magnetic properties of CoCrFeNi high-entropy alloy powders

Presented By: CHIBI Mohamed Ayoub

TOUATI Hamza

Supervisors: Dr. Dadda Karima (USTHB)

Dr. Elmohri Abdennour (Medea Univ)

Academic Year: 2024/2025

Thanks and gratitude

الصلاة والسلام على من لا نبي بعده سيدنا محمد صلى الله عليه وسلم وعلى آله وصحبه اجمعين

Praise be to God, as befits His majesty and great power, who has illuminated for us the path of knowledge and learning, given us the ambition and patience to perform this duty, and enabled us to accomplish this work.

We extend our sincere thanks and gratitude to the entire administrative staff of Dr. Yahya Fares University in Medea, the administrative staff of the faculty of mechanical engineering, and the administrative staff of Badji Mokhtar University in Annaba espicialy Prof; S; Alleg and Dr. N. Dadda for their assistance, support, regular follow-up, and attention to the smallest details.

We must not forget to mention Dr. Elmohri Abdennour and Dr. Dadda Karima for all the support, guidance and accompaniment they provided us throughout the journey of completing this modest work.

MANY THANKS!

Dedication

بسم الله الرحمان الرحيم

(¤ قل اعملوا فسيرى الله عملكم ورسوله والمؤمنون¤)

Oh God, the night is not good except by thanking You, the day is not good except by obeying You, the moments are not good except by remembering You, the hereafter is not good except by Your forgiveness, and Paradise is not good except by seeing You. All praise and thanks are due to You, by Your grace good deeds are accomplished

(Allah, the Almighty, the Majestic)

To those whom God has crowned with awe and dignity, to those who have taught us to give without expectation, to those we cherish with pride. We walk the paths of life, and there remains one who dominates our minds in every path we take.

(Parents)

Stand up for the teacher and honor him The teacher is almost a prophet. Stand tall and embrace the stars There it is enough pride for you to be a teacher. So I say in praise of the teacher, I wonder... Are there any letters left for praise and a book? Everything that has been said in your praise is incomplete... You are the highest and everything else is a mirage.

(DADDA Karima & ELMOHRI Abdennour)

CHIBI Mohamed Ayoub

بسم الله الرحمن الرحيم

✧ إهداء ✧

الحمدُ للهِ الذي بنعمتِهِ تتمُّ الصَّالحات، حمداً يليقُ بجلالِ وجهِهِ، وعظيمِ سلطانِهِ، خلقنا لعبادته، وأمرنا بتوحيده ، والصَّلاةُ والسَّلامُ على خيرِ الأنام، محمَّدٍ وعلى آلهِ وصحبِهِ أجمعين.

- ❖ ***إلى أمّي الحبيبة:*** يا مَن كان دعاؤكِ سرَّ توفيقي، ورضاكِ مطلعَ بركتي، يا من سكنتِ القلبَ حنانًا، وغمرتِ العمرَ عطاءً، جزاكِ اللهُ عنِّي خيرًا، ورفع قدركِ في الدُّنيا والآخرة.
- ❖ ***وإلى أبي العزيز:*** يا مَن علمتني الرجولةَ بثباتِك، والصَّبرَ بحكمتِك، أسألُ الله أن يرزقني برَّك ما حييت، وأن يجزيك خير الجزاء.
- ❖ ***وإلى عائلتي الكريمة الشامخة:*** عائلة **"تواتي"**، نبراس الفضلِ، ومعدن الأصالة، لكم منِّي كلُّ الحبِّ والتقديرِ، أسأل الله أن يديم عزَّكم، ويزيدكم رفعةً وشرفًا.
- ❖ ***وإلى إخوتي الثلاثة و أختي:*** سندي وفخري، من علموني القوة، وكنتم دومًا الحائط الذي لا يميل ,مهما عصفت بي الأيام .
- ❖ ***وإلى أصدقائي:*** رفقاءَ الدربِ، ونِعمَ المعين في الطَّريق **راؤول، محمد، أنس، رياض، يزيد، أيمن**، وكل من جمعني بهم الخير، لكم دعائي بالمحبة الدائمة، والوفاء الصادق.

اللهم اجعل هذا التخرج بداية كل خير، وبارك لي فيه، وانفعني به.

Hamza Touati

Abstract:

$CoCrFeNiAl_x$ (x = 0, and 1 mol, named as Al0, and Al1.0, respectively) high-entropy alloys were mechanically alloyed for 24 h. X-ray diffraction, scanning electron microscopy, and vibrating sample magnetometry investigated crystal structure, microstructure, and magnetic properties. During the milling process, a dual FCC + BCC solid solution with a crystallite size of 15–34 nm was formed. The saturation magnetization (Ms), coercivity (Hc), and squareness ratio (Mr/Ms) have been estimated from hysteresis loops. The Ms values diminished as a result of promoting the formation of the FCC solid solution by the Al addition.

Keywords: High-entropy alloys; Powders; XRD; SEM; VSM

الملخص:

بالطحن الميكانيكي عالي الطاقة لمدة 24 ساعة تم إنتاج سبائك عالية الإنتروبيا من نوع

$CoCrFeNiAl_x$ ($x = 0$ و1 mol) وتمت تسميتها على التوالي Al0 و Al1.0

تم دراسة البنية البلورية، البنية المجهرية، والخصائص المغناطيسية باستخدام الأشعة السينية XRD ، والمجهر الماسح الإلكتروني SEM ، ومغناطومتر العينة المهتزة VSM. أثناء عملية الطحن، تكوّنت محاليل صلبة مزدوجة من نوع FCC + BCC بحجم بلوري يتراوح بين 15–34 نانومتر. قيم الحقل القسري Hc ، مغنطة التشبع Ms ، ونسبة التربيع Mr/Ms تم قياسها باستخدام حلقات التباطؤ. قد كشفت النتائج أن قيم مغنطة التشبع تناقصت نتيجة تعزيز تكوُّن المحلول الصلب من نوع FCC بعد إضافة الألمنيوم.

الكلمات المفتاحية: سبائك عالية الإنتروبيا، مساحيق، XRD; SEM; VSM

Table of contents

Abstract i

List of Figures iii

List of Tables iv

General Introduction

General Introduction 1

Reference 3

Chapter 1: Bibliography

I.1. Nanomaterials 4

I.2. Classification of nanomaterials 4

I.2.1. Classification based on the structural configuration/composition 4

I.2.2. Classification based on dimensions 4

I.2.3. Classification based on pore dimensions 4

I.2.4. Classification based on origin 5

I.2.5. Classification based on potential toxicity 5

I.3. Properties of Nanomaterials 6

I.3.1. Physical properties 6

I.3.2. Magnetic properties 6

I.3.3 Optical properties 6

I.3.4. Electrical properties 7

I.3.5. Chemical properties 7

I.3.6. Mechanical properties 7

I.4. HEAs' Properties based on prior research 7

I.4.1. Electrical properties 7

I.4.2. Magnetic properties 8

I.4.3. Thermal properties 8

I.4.4. Mechanical properties 8

I.5. Functional properties of HEAs 9

Rrference 11

Chapter 2: Experimental Methods

II.1. Synthesis via High-Energy Milling 12

II.1.1. Fundamentals of Mechanical Milling 12

II.1.2. Milling Parameters 14

II.1.2.1. Nature of the starting materials 14

II.1.2.2. Milling Energy (Kinetics) 14

II.1.2.3. Internal Atmosphere of the Jars 14

II.1.2.4. Milling Duration 14

II.1.2.5. Ball-to-Powder Mass Ratio 15

II.1.2.6. Powder Contamination 15

II.1.2.7. Types of Milling Machines 15

II.1.2.8. Milling Temperature 17

II.2. Characterization Techniques 17

II.2.1. X-Ray Diffraction (XRD) 17

II.2.2. Scanning Electron Microscopy (SEM) 20

II.2.3. Vibrating Sample Magnetometer (VSM) 20

Reference 22

Chapter 3: Results &Discussion

III.1. Sample preparation by mechanical alloying 23

III.2. Structural and microstructural properties **24**

III.2.1. X-ray diffraction analysis **24**

III.2.2. SEM analysis **28**

III.3. Magnetic properties **29**

Reference **31**

General Conclusion

General Conclusion **32**

List of Figures

N°	Title	Page
	Chapter 1	
Figure I.1	*General classification of nanomaterials*	5
Figure I.2	*Maximum and minimum hardness of the most studied HEA systems*	9
	Chapter 2	
Figure II.1	*Gridding jars*	13
Figure II.2	*Milling Mechanism*	13
Figure II.3	*Planetary Mill*	16
Figure II.4	*Attritor Mill*	16
Figure II.5	*Reflection of X-rays by a family of lattice planes spaced at a distance d*	18
Figure II.6	*PANalytical Empyrean diffractometer (LM2S Laboratory, UBMA Annaba)*	19
Figure II.7	*SEM QUANTA 250 (ENSMM, Annaba)*	20
Figure II.8	*VSM Lakeshore type 7404 (LM2S Laboratory, UBMA Annaba)*	21
	Chapter 3	
Figure III.1	*Instruments employed in the powders' elaboration*	23
Figure III.2	*XRD patterns of the milled Al0 and Al1.0 powders for 24 h*	24
Figure III.3	*Rietveld refinement of the ball-milled Al0 and Al1.0 powders for 24 h*	25
Figure III.4	*SEM photos of the ball-milled Al0 and Al1.0 powders*	29
Figure III.5	*Hysteresis loops of the ball-milled Al0 and Al1.0 powders*	30

List of Tables

N°	Title	Page
	Chapitre 1	
Table I.1	HEA and their Favourable Features	10
	Chapter 2	
Table II.1	Comparison of different mills	17
	Chapter 3	
Table III.1	Characteristics of the starting Al, Cr, Fe, Co, and Ni elements: atomic radii (r), Valence Electron Concentration (VEC), melting temperature (T_m), crystal structure, activation energy (Q), and enthalpies of mixing for binary pairs of the multicomponent alloy (ΔH_{mix})	26
Table III.2	Lattice parameter, a, crystallite size, <L>, micro strains $<\sigma^2>^{1/2}$, and weight fractions obtained from the Rietveld refinement of the XRD patterns of the ball-milled Al0 and Al1.0 HEAs for 24 h	27

N

General Introduction

For several decades, the development and improvement of nanomaterial synthesis methods have gained much attention among researchers and engineers. Indeed, getting materials of nanometric scale with controlled size and shapes is crucial for several applications in different fields.

Nowadays, nanomaterials are on the way to forming the heart of the next industrial generation since the discovery and development of the atomic force microscope (AFM). This microscope explores matter down to the dimensions of the atom. A high-resolution scanning analysis microscope allows imaging, measuring, and manipulating surfaces at the nanometer scale. This finding has made the universe of nano-materials and their reality more palpable. At this scale, the behavior of matter gives rise to new fundamental mechanical, structural, optical, electronic, and magnetic properties that differ significantly from those observed in bulk materials [1]. These unique properties emerge due to quantum confinement effects, high surface-to-volume ratio, and dominance of negligible interatomic interactions at larger scales. This occurrence opens up vast possibilities for advancements in nanotechnology, paving the way for innovations in medicine, renewable energy, advanced electronics, and materials engineering.

Scientific research has exceeded the conventional alloys based on two or three components to explore the multicomponent alloy systems, such as high entropy alloys (HEAs), which have gained significant attention since their discovery in 2004 by Cantor et al. [2]. The HEAs are named for the high configurational entropy [3] resulting from the randomness of elements in their solid solution form.

Compared to conventional alloys, HEAs contain multiple principal elements (typically five or more) in various proportions, with each principal element carrying a concentration of 5–35 atomic percentages [4], leading to unique properties; in contrast, conventional alloys rely on a dominant-based metal with minor alloying additions. This high configurational entropy stabilizes solid-phase solutions rather than intermetallic compounds. HEAs can possess solid-solution phases with face-centered cubic (fcc), body-centered cubic (bcc), or hexagonal close-packed (hcp) [5]. One can also add some minor elements with concentrations less than five atomic percentages to enhance the properties of HEAs.

High entropy systems containing Co, Cr, Cu, Fe, Mn, Ni, and Al have been widely studied with varied preparation and processing methods such as arc melting, induction melting,

mechanical alloying, plasma sintering, etc. [6-8]. The wide range and critical nature of their structural, physical, and mechanical properties make them a focal point of ongoing research.

This work aims to elaborate CoCrFeNi and CoCrFeNiAl high entropy alloys by the mechanical alloying technique. Scanning electron microscopy (SEM), X-ray diffraction (XRD), and vibrating sample magnetometer (VSM) have been employed to follow the morphology, microstructure, structure, and magnetic properties of samples to discuss the effect of the Al addition on different properties.

The manuscript contains a general introduction, three chapters, and a general conclusion. The first chapter deals with a bibliographic review of high entropy alloys, their different properties, and application domains. The second chapter is dedicated to the sample preparation and characterization techniques. The third chapter presents and discusses the structural, microstructural, and magnetic properties of the ball-milled CoCrFeNi and CoCrFeNiAl alloys. Finally, the general conclusion summarizes the main results obtained.

1. A. Hamdouche. Structural, Electronic, and Magnetic Properties of Nanometric Compounds. Master's Thesis (2021) University of Mohamed El Bachir El Ibrahimi, Bordj Bou Arréridj.
2. Y.F. Ye, Q. Wang, J. Lu, C.T. Liu, Y. Yang. High-entropy alloy: challenges and prospects. *Mater. Today.* (2016) 19:349-62.
3. Y. Zhang, T.T. Zuo, Z. Tang, M.C. Gao, K.A. Dahmen, P.K. Liaw, Z.P. Lu. Microstructures and properties of high-entropy alloys. *Prog. Mater. Sci.* (2014) 61:1-93.
4. A.O. Moghaddam, N.A. Shaburova, M.N. Samodurova, A. Abdollahzadeh, E.A. Trofimov. Additive manufacturing of high entropy alloys: A practical review. *J. Mater. Sci. Technol.* (2021) 80:171-91.
5. B. Cantor. Multicomponent high-entropy Cantor alloys. *Prog. Mater. Sci.* (2021) 118:100774.
6. P. Dolez, editor. Nano-engineering: Global Approaches to Health and Safety Issues. 1st ed. Amsterdam, Netherlands: Elsevier; 2015.
7. B. Cantor, I.T.H. Chang, P. Knight, A.J.B. Vincent. Microstructure development in equi-atomic multicomponent alloys. *Mater. Sci. Eng. A* (2004) 375–377, 213–218.
8. S.C. Duan, J. Kang, J. Cho, M. Lee, W.Z. Mu, J.H. Park. Manufacturing an ultra-low-sulfur CoCrFeMnNi high-entropy alloy by slagging through induction melting with ferroalloys feedstock. *J. Alloys Compd.* (2022) 928, 167080.
9. D. Yim, M.J. Jang, J.W. Bae, J. Moon, C.H. Lee, S.J. Hong, S.I. Hong, H.S. Kim. Compaction behavior of water-atomized CoCrFeMnNi high-entropy alloy powders. *Mater. Chem. Phys.* (2018) 210, 95–102.

Chapter I

Bibliography

This chapter deals with a bibliographic review of nanomaterials specifically high entropy alloys, their different properties, and application domains.

I.1. Nanomaterials

The prefix Nano comes from the Greek "Nanos" which means "very small". In 1955, it was chosen as a subunit of the meter (1 nm = 10^{-9} m). On the 29th December 1959, in his speech given to the American Physical Society, Richard Feynman opens the way to a then unexplored field of research "the infinitely small". He considered an aspect of physics based on the tiny size of the atoms, where it is feasible to write large amounts of information.

Nanomaterials are defined by the fact that they consist of an assembly of nanometric particles with a size down to 100 nm. They possess a higher concentration of free atoms located at the boundaries of their grains, which leads to improved characteristics or different properties from those of conventional micrometric materials. These changes concern the mechanical, physical (optical, magnetic, and electrical), and chemical properties.

I.2. Classification of Nanomaterials

One can classify nanomaterials depending on their size, place of origin, structural configuration, pore size, and potential toxicity as depicted in Figure I.1.

I.2.1. Classification based on the structural configuration/composition

According to their structural makeup, one categorizes the nanoparticles into four groups: organic/dendrites, inorganic, carbon-based, and composite.

I.2.2. Classification based on dimensions

Based on their dimensions, nanomaterials can be zero-dimensional (0D), one-dimensional (1D), two-dimensional (2D), and three-dimensional (3D) materials.

I.2.3. Classification based on pore dimensions

Nanomaterials are classified into three groups based on the length of their diameter dimensions: micro-porous (pore size < 2 nm), mesoporous (pore size 2–50 nm), and macro-porous (pore size > 50 nm). The size of the pores determines the size of molecules and affects diffusion and interaction properties.

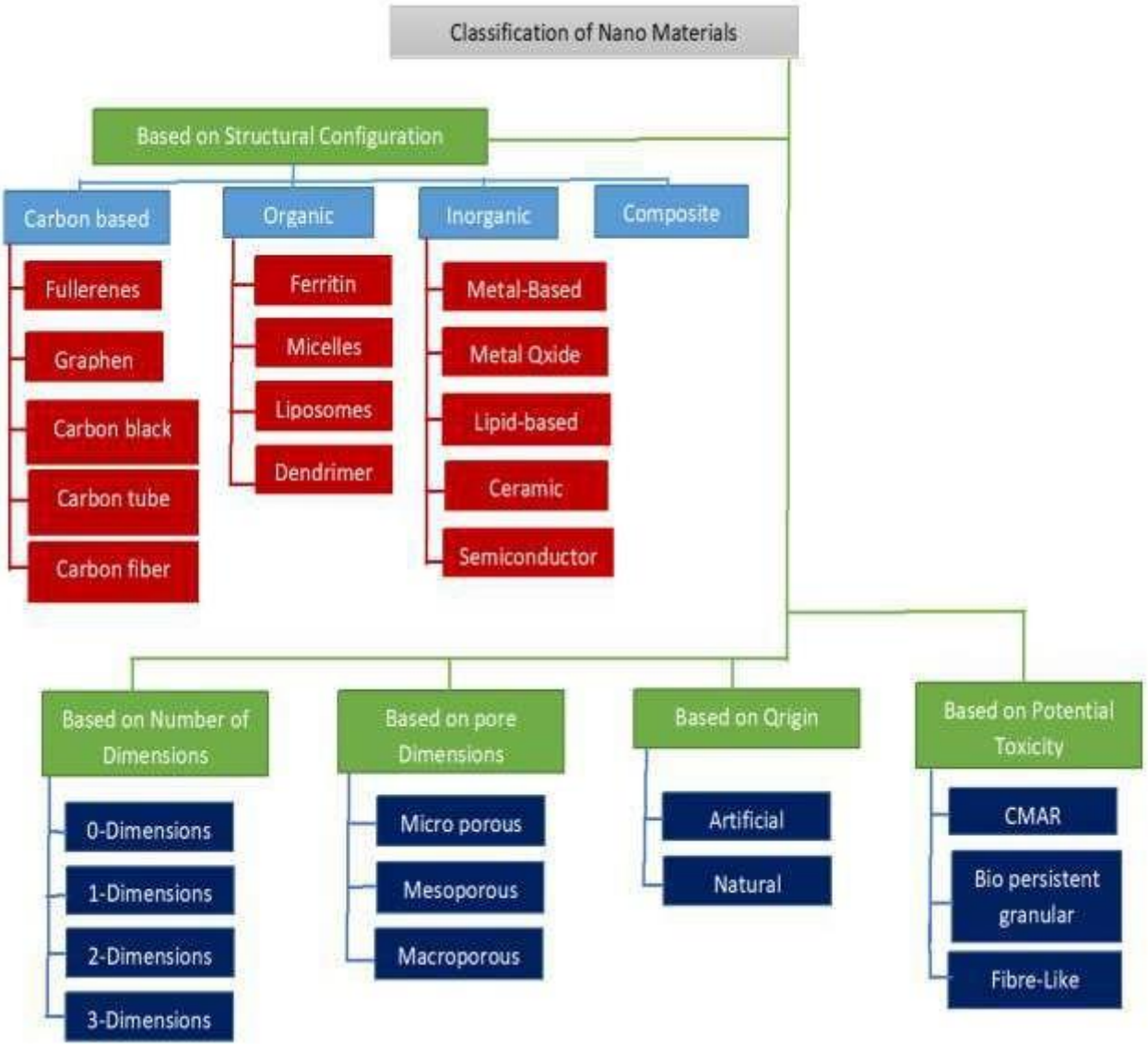


Figure I.1: *General classification of nanomaterials.*

I.2.4. Classification based on origin

Nanomaterials can be divided based on origin into natural nanoparticles, such as volcanic ash, protein molecules, mineral springs, and artificial nanoparticles like carbon nanotubes and semiconductors.

I.2.5. Classification based on potential toxicity

Nanomaterials are classified into three groups based on their toxicity degree (high, moderate, and low toxicity). For instance, highly toxic nanomaterials refer to fibre-like nanoparticles, persistent granular nanoparticles, and CMAR nanoparticles (carcinogenic, mutagenic, asthma-genic, reproductive toxin) [1]. Some metal oxide nanoparticles (e.g., TiO_2, ZnO) are toxic under UV exposure or high doses; they have a moderate toxicity. The

biocompatible nanomaterials exhibit minimal or no harmful effects on biological systems and the environment; they are low-toxic.

I.3. Properties of Nanomaterials

The properties of nanometer-scale materials differ significantly from those of bulk materials due to the crystallography, composition, surface area, and nanoscale size effects, which can be seen in several properties.

I.3.1. Physical properties

The melting temperature of a bulk material is independent of its size. However, the melting point of nanomaterials decreases as the particle size decreases due to the unbounded surface atoms. When subdividing a bulk material into nano-scale materials, its total volume remains unchanged. However, its collective surface area increases. Compared to bulk materials, the increased surface-to-volume ratio at the nano-scale can enhance the catalytic efficiency and surface-dependent properties. The surface molecules of orators have a high surface energy and a proclivity to agglomerate, affecting the structural, microstructural, and morphological properties.

I.3.2. Magnetic properties

The magnetic behavior of elements can change according to the size of magnetic nanoparticles, leading to soft or hard magnets with improved properties such as coercivity. Non-magnetic bulk materials can become magnetic at the nano-scale. For example, gold and platinum are non-magnetic in bulk but magnetic on the nano-scale.

I.3.3 Optical properties

Localized surface Plasmon resonance (LSPR) is an optical property of nanoparticles. Some studies have shown that by decreasing the size of Au nanoparticles, the emission light position changes from the near-infrared (NIR) region to the ultraviolet (UV) region. Due to their small size, nanoparticles can lose their LSPR and become photo-luminescent [2].

Furthermore, matter can change color at the nano-scale; for example, gold nano-spheres can turn yellow at 100 nm, greenish-yellow at 50 nm, and red at 25 nm, while silver can also turn orange at 200 nm, light blue at 90 nm, and blue at 40 nm spherical thin film length [3].

I.3.4. Electrical properties

Nanomaterials can increase conductivity in ceramics but increase electric resistance in metals. Electron conduction is delocalized in bulk materials, which means electrons can move freely in all directions. When the scale is reduced to the nano-scale and due to electron confinement, the energy bands are replaced by discrete energy states, causing conducting materials to behave as semiconductors or insulators. This result indicates that the metal is becoming a semiconductor.

I.3.5. Chemical properties

The stability and sensitivity of the nanoparticles to elements such as moisture, environment, heat, and light significantly influence their performance and potential applications. The flammability, corrosiveness, anti-corrosiveness, oxidative potential, and reduction potential of nanoparticles all play a role in determining their applications [4]. Nanomaterials exhibit significantly improved or novel catalytic properties, such as enhanced reactivity and selectivity, compared to their bulk counterparts [5].

I.3.6. Mechanical properties

The mechanical properties of materials, such as elasticity, ductility, tensile strength, and flexibility, play crucial roles in their application. Influence on mechanical properties in nanomaterials, such as increased hardness, yield strength, elastic modulus, and toughness compared to bulk materials. The strength and hardness of nanostructured materials increase with decreasing grain size and grain boundary deformation [6].

I.4. HEAs' Properties based on prior research

Because components are usually more localized in HEAs than traditional alloys, regardless of the same alloy family, changing just one element can considerably affect the microstructure and electrical, magnetic, mechanical, and thermal properties.

I.4.1. Electrical properties

For the same composition, the fcc-phase has a larger electrical resistivity than the bcc-phase. For instance, the electrical resistance of $Al_xCoCrFeNi$ alloys (0×2) rises with a linear trend with temperature. A non-monotonic electrical resistivity dependence could result from the microstructures switching from "fcc" to "bcc" as the Al content rises [7].

I.4.2. Magnetic properties

Investigations on the magnetic characteristics of HEAs have mainly concentrated on alloys made of Cr, Co, Al, Cu, Ni, Ti, and Fe. Higher magnetization often results in more magnetic elements. However, adding components to alloys can have a considerable influence. For example, the magnetization is decreased when Cr is added. Similarly, to conventional magnetic materials, higher coercivities are associated with finer microstructures. Miracle et al. [8] reported that as-processed materials often exhibit distinct microstructures and magnetic characteristics compared to annealed ones.

I.4.3. Thermal properties

Thermal conductivity is frequently determined by measuring a material's density, specific heat, and thermal diffusion coefficient. The region with the lowest thermal conductivity is the fcc + bcc duplex. However, low Al concentration single-phase fcc alloys have a thermal conductivity almost half that of high Al content (single-phase bcc alloys). Specifically, the increased Al concentration in single-phase zones implies lower thermal conductivity, which is mainly caused by lattice distortions and the improved phonon mean free path brought on by lattice thermal expansion at elevated temperatures [9].

I.4.4. Mechanical properties

One can highlight that the composition and microstructure significantly influence the mechanical characteristics. Defects are crucial for alloys' microstructure and considerably affect the mechanical properties. Meanwhile, the composition determines the elastic characteristics and atomic interactions that manage the dislocation behaviors [10]. Besides, it is essential to recap that the alloy's hardness depends on its constituent parts and their interaction. Yeh et al. reported that HEA has variable compressive behavior depending on temperature and strain rate. Figure I.2 depicts that most HEAs have more hardened surfaces than standard alloys [11].

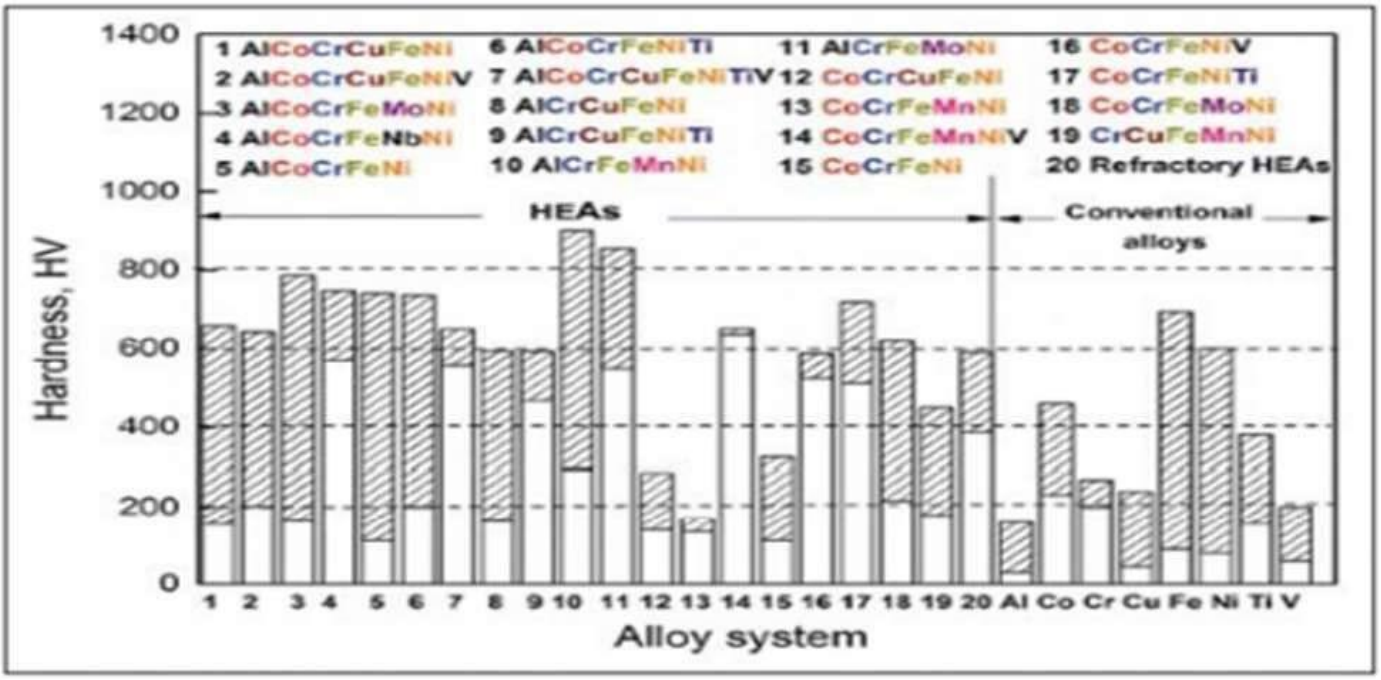


Figure I.2: *Maximum and minimum hardness of the most studied HEA systems [11].*

I.5. Functional properties of HEAs

For instance, HEAs show great interest in their mechanical and microstructural characteristics. Meanwhile, focusing on their functional abilities, HEAs display mingled properties of soft-magnet, radiation resistance, thermoelectric, and catalytic qualities. These functional characteristics depend on their unique multi-principal element solid solution structure and are crucial for numerous applications such as electromagnetic interference shielding, nuclear magnetic resonance, and solar plates. Table I.1 summarizes some prospective applications of HEAs in different fields [12].

Table I.1: HEA and their Favourable Features

HEA	Favorable Features
Solar absorber coating	Excellent absorption capacity, robust corrosion resistance, high-temperature mechanical properties, and exceptional strength and hardness.
Diffusion barrier films	Exceptional thermal stability and diffusion resistance.
Aviation and turbine manufacturing (engine components, steam turbine blades, boiler pipes, heat exchanger tubes, aero engine components)	High efficiency, high solubility, hardness, great thermal stability, high-pressure, high-temperature materials, superconductivity and low density, outstanding cold formability and high strength-to-weight ratio.
Components of a nuclear reactor	Ion irradiation resistance, creep resistance, less radioactive waste, and higher temperature strength.
Marine ship vessel	Low specific energy requirements, improved workability, and the design of HEAs with high melting points.
Coating in the automobile sector	Higher bond strength, no phase shift, excluded aggregation, and a lower wear rate.
Tools and high-temperature applications	Larger ingots, higher purity, less energy use, and greater microstructural control.
Coatings	High-temperature oxidation, hot corrosion resistance, and thermal stability.
The automotive and tiny electronics sector	Better surface finish, quick and effective.
Welding	Better mechanical strength, low porosity.
Aerospace	High stress and high-temperature resistance.
Biomedical materials (biological equipment, bio-ceramic materials)	Excellent wear qualities, chemical stability, high hardness, strong biocompatibility, and high stiffness.

1. P. Dolez, editor. Nanoengineering: Global Approaches to Health and Safety Issues. Elsevier, Amsterdam, Netherlands, 2015.
2. K.H. Huynh, X.H. Pham, J.Kim, S.H.Lee, H. Chang, W. Rho, B.H. Jun. Synthesis, Properties, and Biological Applications of Metallic Alloy Nanoparticles. *Int. J. Mol. Sci.* (2020) 21: 5174.
3. S. Horikoshi, N. Serpone, editors. Microwaves in Nanoparticle Synthesis: Fundamentals and Applications. Germany: John Wiley & Sons; 2013.
4. I. Ijaz, E. Gilani, A. Nazir, A. Bukhari. Green synthesis of metallic nanoparticles using plant extracts. *Green Chem. Lett. Rev.* (2020) 13:223-45.
5. H.M. Yusuf, N.A. Rahman, R. Mohamad, U.H. Zaidan. Microbial Mediated Synthesis of silver Nanoparticles by Lactobacillus Plantarum TA4 and its Antibacterial and Antioxidant Activity. *Appl. Sci*. (2020) 10:6973.
6. G. Cho, Y. Park, Y.K. Hong, D.H. Ha. Recent advances in high-entropy alloys for biomedical applications. *Nano Converg.* (2019) 6:35.
7. J. Chen, X. Zhou, W. Wang, Y. Liu. A review on fundamentals of high entropy alloys with promising high–temperature properties. *J. Alloy. Compd.* (2018) 766:1031-46.
8. D.B. Miracle, O.N. Senkov. A critical review of high entropy alloys and related concepts. *Acta Mater.* (2017) 122:448-511.
9. V. Chaudhary, R. Chaudhary, R. Banerjee, R.V. Ramanujan. Accelerated and conventional development of magnetic high-entropy alloys. *Mater. Today* (2021) 45:131-51.
10. A. Gali, E.P. George. Tensile properties of high- and medium-entropy alloys. *Scripta Mater.* (2013) 69:37-42.
11. P. Yang, Y. Liu, X. Zhao, J. Cheng, H. Li. Electromagnetic wave absorption properties of mechanically alloyed FeCoNiCrAl high-entropy alloy powders. *J. Magn. Magn. Mater.* 2016; 401:72-6.
12. A. Gali, E.P. George. Tensile Properties of high- and medium-entropy alloys. *Intermet.* (2013) 39: 74-78.

Chapter II

Experimental Methods

This chapter outlines the methodology for developing the studied system and presents the various characterization techniques employed. The analysis of the obtained diffractograms is carried out using the MAUD refinement program.

II.1. Synthesis via High-Energy Milling

High-energy milling, also known as mechanosynthesis, is a technique that enables the synthesis of nanostructured materials at room temperature. It is often hard to produce such materials using traditional methods like melting or physical vapor deposition (PVD). Initially developed in the late 1960s for the fabrication of oxide-dispersed nickel-based alloys (Al_2O_3, Y_2O_3) used in gas turbines, this process has since gained widespread attention. It enables the creation of various non-equilibrium materials, including amorphous alloys, supersaturated solid solutions from immiscible or partially miscible elements, quasicrystals, and disordered metallic alloys [1-3].

Despite its relatively low energy efficiency, the mechanosynthesis method offers a pathway for scaling up from laboratory to industrial production. Depending on the type of milling equipment used, powder mixtures ranging from just a few grams (10 g) to large-scale batches of up to one ton can be processed.

II.1.1. Fundamentals of Mechanical Milling

High-energy milling involves the vigorous agitation of powder, consisting either of pure elements or of pre-alloyed materials, together with milling balls inside a hermetically sealed stainless-steel container (jar), as depicted in Figure II.1. The repeated collisions between the balls and the powder particles induce a series of plastic deformations, fracturing, and cold-welding events. This process leads to the progressive refinement of the powder grains, ultimately resulting in the formation of a fine and homogeneous mixture [1, 3, 4].

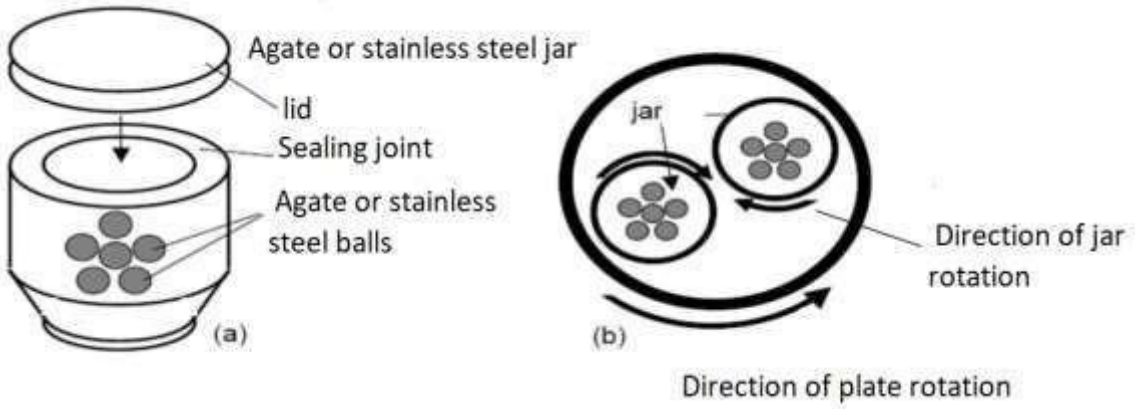


Figure II.1: *Gridding jars [5].*

During each collision, a portion of the powder (around 1000 particles) is trapped between balls, absorbing elastic energy. The impact force deforms the particles, causing them to fracture (Figure II.2). The newly generated surfaces subsequently undergo re-welding [6]. The interplay between these two processes, fracture and welding, determines whether the particles grow or decrease in size, depending on the ductility or brittleness of the agglomerated powders.

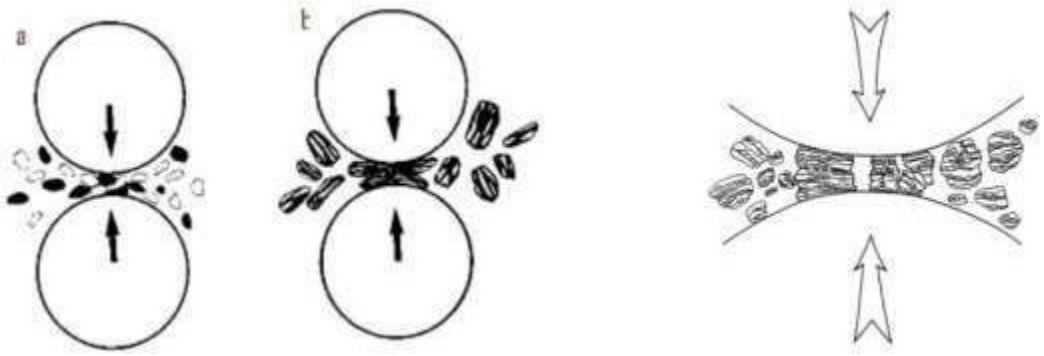


Figure II.2: *Milling Mechanism [4].*

During the milling process, the powder experiences intense plastic deformation, resulting in a higher defect density within the crystal lattice and an increase in temperature. The kinetic energy transfer drives this temperature rise between the milling balls and the powder particles, facilitating the formation of solid solution regions.

II.1.2. Milling Parameters

II.1.2.1. Nature of the starting materials

The structural characteristics, particle size, miscibility of the elements, and initial composition of the powder mixture play a crucial role in determining the size, shape, and morphology of the final product. Depending on the nature of the starting materials. One can identify three types of powder mixtures:

- **Ductile–Ductile Systems:** In the initial milling phase, powder particles undergo flattening due to micro forging. These flattened particles weld together, forming a layered (lamellar) structure. As milling time progresses, diffusion distances shorten, and defect density increases, enhancing the homogenization process.
- **Ductile–Brittle Systems:** The ductile particles flatten, while the brittle particles fragment and become embedded within the ductile matrix. With extended milling, a lamellar structure develops, where brittle fragments distribute uniformly if they are insoluble. If solubility exists between the components, they intermix, achieving chemical homogeneity.
- **Fragile–Fragile Systems:** in fragile–fragile systems, brittle particles continuously fragment, leading to a progressive reduction in particle size over time until reaching a critical size. Therefore, the most fragile ones will be smashed and become embedded within the remaining particles [6, 7].

II.1.2.2. Milling Energy (Kinetics)

The milling energy is directly related to the movement speed of the milling jars, whether through rotation or vibration. For example, a higher milling speed accelerates the formation of the final product.

II.1.2.3. Internal Atmosphere of the Jars

To prevent contamination, inert gases such as argon (Ar) or helium (He) are typically used. However, when producing oxides, nitrides, or hydrides, reactive gases such as air, nitrogen (N_2), or hydrogen (H_2) can be employed.

II.1.2.4. Milling Duration

Milling duration defines the time required to obtain the final product. It depends on several factors, including the type of milling machine, the interaction between the milling balls and the

powder (elastic collisions or friction), the nature of the powder, and temperature control during milling. Continuous milling may lead to a different product compared to milling with intermittent pauses [8].

II.1.2.5. Ball-to-Powder Mass Ratio

The mass ratio between the milling balls and the powder significantly affects phase formation in the milled material. This ratio can range from 1/1 to 220/1. Increasing the ball-to-powder ratio reduces the time needed to achieve the final product [9]. Using a higher ratio implies more frequent collisions per unit of time with greater energy transfer to the powder, accelerating then the alloy formation [10].

II.1.2.6. Powder Contamination

Powder contamination is influenced by both milling time and intensity, as well as the mechanical properties of the milled material. Contamination from milling tools can be minimized by using jars and milling balls made of materials similar to the powder being processed.

II.1.2.7. Types of Milling Machines

Milling machines vary in terms of operating principles, energy input, and capacity. Common types include planetary mills, attractors, and vibratory mills, each offering different advantages depending on the application.

- **Planetary Mill:** In this type of mill, a set of milling balls (typically 1 to 2 cm in diameter) is placed inside a chamber along with the powder. The chamber itself is mounted on a rotating disk that spins in the opposite direction (Figure II.3). Common planetary mills include the Fritsch Pulverized P0, P5, and P7, with capacities ranging from 10 to 250 cm^3.

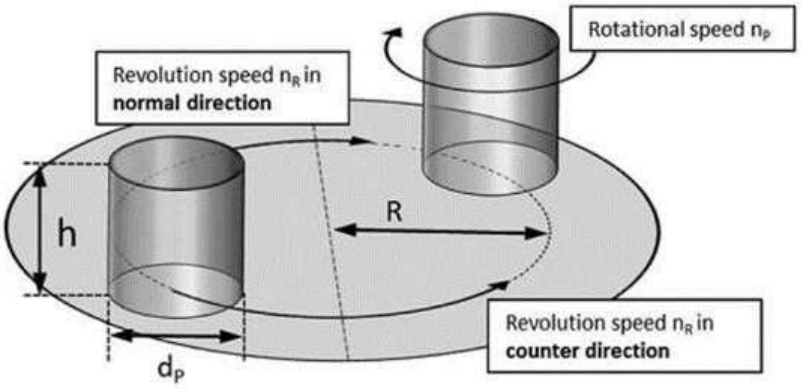


***Figure II.3**: Planetary Mill.*

- **Vibratory Mill:** Here, the milling balls and powder are agitated in three perpendicular directions simultaneously. The SPEX 8000 vibratory mill is the most widely used model. While it provides higher energy input than planetary mills, its capacity remains relatively low.
- **Attritor Mill:** In this system, over 1000 milling balls (0.2 to 1 cm in diameter) are contained within a vertical chamber, agitated by rotating elements fixed to a central shaft. Attritor mills have a significantly larger capacity, ranging from 0.5 to 100 kg (Figure II.4). Table II.1 provides a comparative summary of the properties of these different milling machines.



***Figure II.4:** Attritor Mill.*

Table II.1: Comparison of different mills [11]

	Attritor	**Planetary**	**Vibratory**
Number of balls	< 1000	5-12	4-12
Ball diameter (mm)	2-10	10-20	10
Ball movement	Rolling	Rolling + Impact	Impact
Ball speed (m/s)	0-0.8	2.5-4	-
Kinetic energy (10^2J/ball)	< 1	1-40	< 12
Impact frequency (Hz)	> 1000	100	200
Power (W/g.ball)	< 0.001	0.01-0.8	< 0.24
Average temperature (°C)	150	50-120	60

II.1.2.8. Milling Temperature

In high-energy milling, two types of temperatures are considered: local and macroscopic temperatures. The local temperature refers to the temperature of powder particles undergoing intense shear forces, and the macroscopic one represents the average temperature of the milling tools (jar and balls). The temperature rise during milling can be beneficial in certain cases, as it enhances diffusion, promoting homogenization and alloy formation. However, excessive temperature increases can have adverse effects, such as triggering phase transformations, decomposing supersaturated solid solutions or metastable phases formed during milling, or even crystallizing an amorphous phase.

II.2. Characterization Techniques

II.2.1. X-Ray Diffraction (XRD)

X-ray diffraction (XRD) is a powerful technique for analysing the crystal structure of materials. It provides information about crystallite size, macro strain levels, atomic positions, and phase identification. The identification of crystalline phases is based on measuring the

intensity and position of diffraction peaks. The determination of atomic positions allows for the calculation of interlunar distances (d_{hkl}) using Bragg's law (Figure II.5):

$$2d_{hkl}\, sin\theta = n\lambda \qquad \text{(II.1)}$$

Where θ is the angle of the incident X-rays, n is the order of reflection, and λ is the wavelength of the incident X-rays.

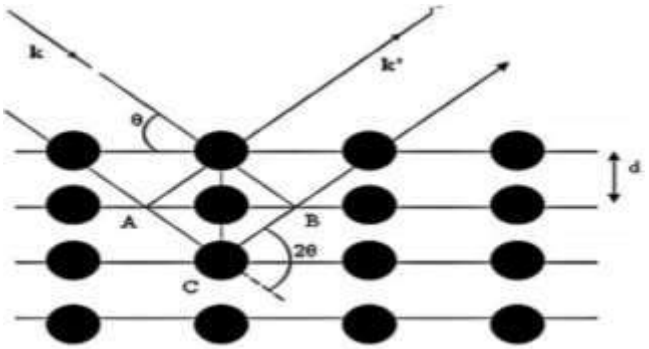


Figure II.5: *Reflection of X-rays by a family of lattice planes spaced at a distance d.*

The X-ray diffractograms were recorded using the PANalytical Empyrean diffractometer in Bragg-Brentano geometry ($\theta - 2\theta$) over the angular range of 20–80° with a step size of 0.01°. The radiation used was Cu with a wavelength of $\lambda_{Cu}(K\alpha) = 1.54056$ Å. The diffractograms were refined using the Rietveld method with the MAUD (Materials Analysis Using Diffraction) software [12, 13], which is based on the Rietveld refinement technique.

The Rietveld method is a structural refinement technique that involves simulating a diffractogram based on a structural model and adjusting the parameters until the simulated and measured diffract grams overlap, by minimizing the least squares of the following equation:

$$M = \sum w_i\,(y_i - y_c)^2 \qquad \text{(II.2)}$$

where y_i and y_{ci} are, respectively, the values of the intensities measured and calculated in step i and $w_i = 1/y_i$ is the weight associated with the intensity y_i:

$$y_i = y_{iBF} + hs \sum_h L_h |F_h|^2\, G\,(2\theta_i - 2\theta_h)\, A_h P_h \qquad \text{(II.3)}$$

with y_{iBF}: Intensity of the continuous background; h: Multiplicity of reflection; s: The scale factor; L_h: Factor of Lorentz and polarization; F_h: Factor structure; G: Function profile of the reflection h; $2\theta_i$ is the angle of diffraction; $2\theta_h$: the angle of diffraction for the reflection h;

A_h: Function of asymmetry; and P_h: Function describing the preferential orientation of the crystallites.

The quality of the refinement is given by several factors including the parameter χ^2 or goodness of fit, which must tend towards 1:

$$\chi^2 = \frac{\text{Rwp}}{\text{R exp}} \qquad \text{(II.4)}$$

Hence, the weighted (R_{wp}) and experimental (R_{exp}) profile factors are defined by:

$$R_{wp} = \left[\frac{\sum(y_i - y_{ci})^2}{\sum w_i y_i^2}\right]^{1/2} \qquad \text{(II.5)}$$

$$R_{exp} = \left[\frac{N-P}{\sum w_i y_i^2}\right]^{1/2} \qquad \text{(II.6)}$$

where y_i is the intensity measured at the i^{the} step and y_{ci} the intensity calculated at the i^{the} step of the diagram $w_i = 1/y_i$; N the number of points of the experimental diffraction diagram; and P the number of refined parameters.

The average size of the crystallite size $\langle L \rangle$ is inversely proportional to the total enlargement of the Bragg peak and is given by Scherer's formula:

$$\langle L \rangle = \frac{\lambda}{\mathcal{L}.\cos\theta} \qquad \text{(II.7)}$$



Figure II.6: *PANalytical Empyrean diffractometer (LM2S Laboratory, UBMA Annaba).*

II.2.2. Scanning Electron Microscopy (SEM)

Scanning Electron Microscopy (SEM) is based on the principle of electron-matter interaction, allowing the production of high-resolution images of a conductive sample surface. Electrons emitted from a heated filament due to thermoelectric effects are accelerated by a potential difference and then scanned across the observed surface in two directions. Multiple detectors collect the emitted electrons, enabling the reconstruction of a three-dimensional image of the surface. This results in an atomic number contrast image produced by backscattered electrons and a topographic contrast image generated by secondary electrons.

The morphology of the powders was studied using a QUANTA 250 scanning electron microscope, with an image resolution of 3584 × 3094 pixels (16 bits), magnification up to 20000 times, an analysis depth in the micrometer range, and a minimum analysable size in µm (Higher National School of Mines and Metallurgy, Annaba).



Figure II.7: *SEM QUANTA 250 (ENSMM, Annaba).*

II.2.3. Vibrating Sample Magnetometer (VSM)

The magnetic hysteresis loop is obtained using a Vibrating Sample Magnetometer (VSM), which allows the determination of saturation magnetization, remnant magnetization, and coercive field. Its operating principle is based on the flux method, where the sample vibrates vertically at a fixed frequency and a constant amplitude, generating a variation in magnetic flux within the measurement coils. This flux variation is proportional to the sample's magnetization,

inducing an electromotive force (EMF). By applying a constant magnetic field, the magnetization of the material can be calculated as a function of the applied magnetic field, which is generated by an electromagnet. For measurements, a 40 mg powder sample is packed inside a transparent plastic diamagnetic capsule, which is suspended from a rod inside the VSM chamber. The measurements were conducted at T = 300 K under a magnetic field of 2 T (20 kOe).



Figure II.8: *VSM Lakeshore type 7404 (LM2S Laboratory, UBMA Annaba).*

1. E. Gaffet, L-C. Gérard. Mechanical processing for Nanomaterials. *En. Nanosci. Nanotechnol.* (2004) 5: 91-129.
2. E. Gaffet, M. Harmelin. Crystal-amorphous phase transition induced by ball-milling in silicon. *J. Less Common Metals* (1990) 157: 201-222.
3. C. Suryanarayana. Mechanical alloying: a novel technique to synthesize advanced materials. *Research* (2019) 10: 1-17.
4. S. Galdeano. Influence of milling conditions on the distribution of magnetic nanoparticles (Fe, Co) in a copper matrix. PhD dissertation (2001) University of Paris 7.
5. M. Grafoute. Study of the structural properties and modeling of nanostructured iron powders obtained by mechanical milling. PhD dissertation (2004) University of Le Mans.
6. C. Suryanarayana, Cury. Mechanical alloying and milling. *Progress Mater. Sci.* (2001) 46: 1-184.
7. S. Alleg, S. Souilah, J.J. Suñol. Thermal stability of nanostructured powder mixtures prepared by mechanical alloying. In Applications of Calorimetry in a Wide Context - Differential Scanning Calorimetry, Isothermal Titration Calorimetry, and Microcalorimetry. *Intech Open* (2013).
8. P. Florin. Elaboration and study of soft magnetic powders (Ni-Fe, Ni-Fe-X, Ni-Fe-XY) in a nanocrystalline state by high-energy mechanical milling. PhD dissertation (2008) University of Joseph-Fourier-Grenoble I.
9. C. Suryanarayana, A. Nasser. Mechanically alloyed nanocomposites. *Progress Mater. Sci.* (2013) 58: 383-502.
10. C. Suryanarayana. Mechanical alloying and milling. Marcel Dekker Inc., (2004).
11. Suryanarayana C. Mechanical alloying and milling. Progress in Materials Science. 2001;46(1):1–184. doi:10.1016/S0079-6425(99)00010-9.
12. L. Lutterotti, S. Matthies, H. Wenk. MAUD (Material Analysis Using Diffraction): A user-friendly Java program for Rietveld texture analysis and more. In Proceedings of the Twelfth International Conference on Textures of Materials (ICOTOM-12), NRC Research Press, Ottawa, Canada, (1999).
13. L. Lutterotti. "MAUD - Materials Analysis Using Diffraction." (1997).

Chapter III

Results

& Discussion

This chapter is devoted to the presentation and discussion of the results obtained from the mechanically alloyed CoCrFeNi and CoCrFeNiAl powders. The influence of the aluminium content on the structure, microstructure, morphology, and magnetic properties is studied by X-ray diffraction, scanning electrons microscope, and vibrating-sample magnetometer.

III.1. Sample preparation by mechanical alloying

The elemental powders cobalt, chromium, iron, nickel, aluminium were weighed using a highly sensitive electronic balance (METTLER TOLEDO) with a precision of 10^{-4} in order to produce mixtures with a nominal composition of CoCrFeNi and CoCrFeNiAl (at.%), named as Al0 and Al1.0, respectively. The reactants, along with the milling balls, were placed in a 60 ml stainless steel jar under an inert atmosphere inside a glove box filled with purified argon. The jar's lid, equipped with a sealing gasket, was screwed onto the cylindrical body of the jar. The jar was then placed on the platform of a planetary ball mill, model Retsch PM400. Milling was carried out at room temperature for 24 hours using 6 g of the powder mixture with six 12 mm diameter balls (corresponding to a ball-to-powder mass ratio of 12:1). A rotation speed of 400 rpm was selected to promote the "direct impact" mode. The milling was carried out in 30-minute cycles followed by 15-minute pauses. The jars were opened after a cooling period of 15 to 30 minutes.

The various instruments used in the preparation of the powders are shown in Figure III.1.



Figure III.1: *Instruments employed in the powders' elaboration.*

III.2. Structural and microstructural properties

III.2.1. X-ray diffraction analysis

During the milling process, the trapped powder particles between the balls and/or in the ball-wall surface are subjected to severe deformation, fracture, welding, and rewelding depending on the nature of the metallic powders. The total mixing of the elemental powders at the atomic level is evidenced by the disappearance of their diffraction peaks, as shown by the XRD patterns of the mechanically alloyed Al0 and Al1.0 powders for 24 h in Figure III.2. Moreover, the broadening of the diffraction peaks and the decrease in their height are related to the crystallite size reduction and the introduction of an important fraction of structural defects during the milling process, such as vacancies, grain boundaries, dislocations, and so on. Likewise, the peak asymmetry can be related to the structural heterogeneity through the existence of more than a single solid solution. Furthermore, the effect of Al addition is revealed by the shape and position of the main diffraction peak. Accordingly, the phase identification was determined using the MAUD program [01], which is based on the Rietveld method [02]. The structural refinement was achieved with two phases: BCC type (lattice parameter $a_0 = 2.865$ Å, space group Im-3m), and FCC type (lattice parameter $a_0 = 3.528$ Å, space group Fm-3m) as depicted by Figure III.3. For the HEAs, the formation of disordered solid solutions during the milling process is allowed by the proximity of the atomic radii of the constituent components Al, Cr, Fe, Mn, Co, and Ni ($r_{Al} > r_{Cr} > r_{Co} = r_{Ni} > r_{Fe}$), their large negative enthalpies of mixing, and their activation energies (Table 1).

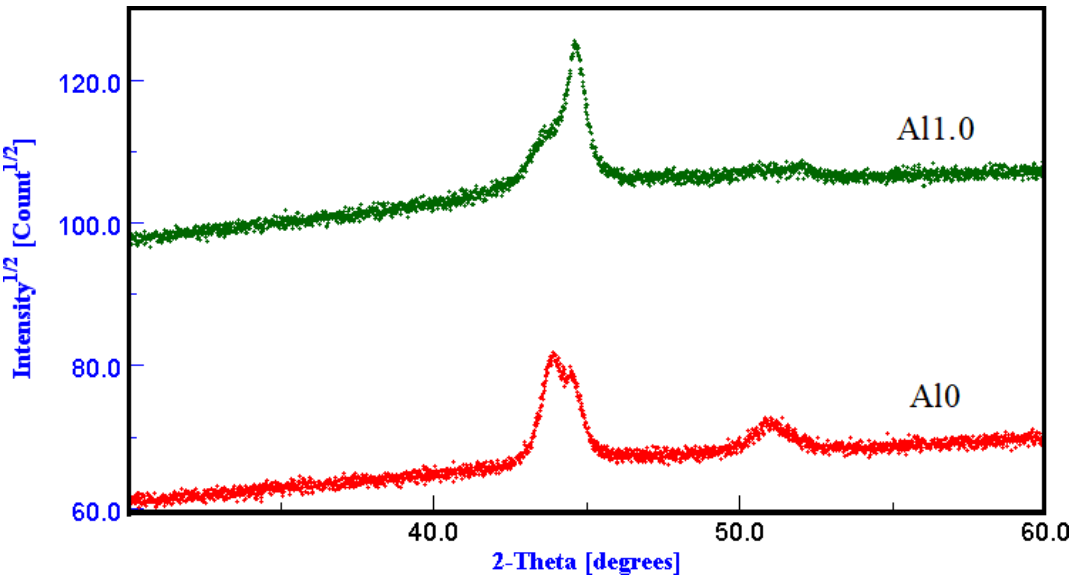


Figure III.2: *XRD patterns of the milled Al0 and Al1.0 powders for 24 h.*

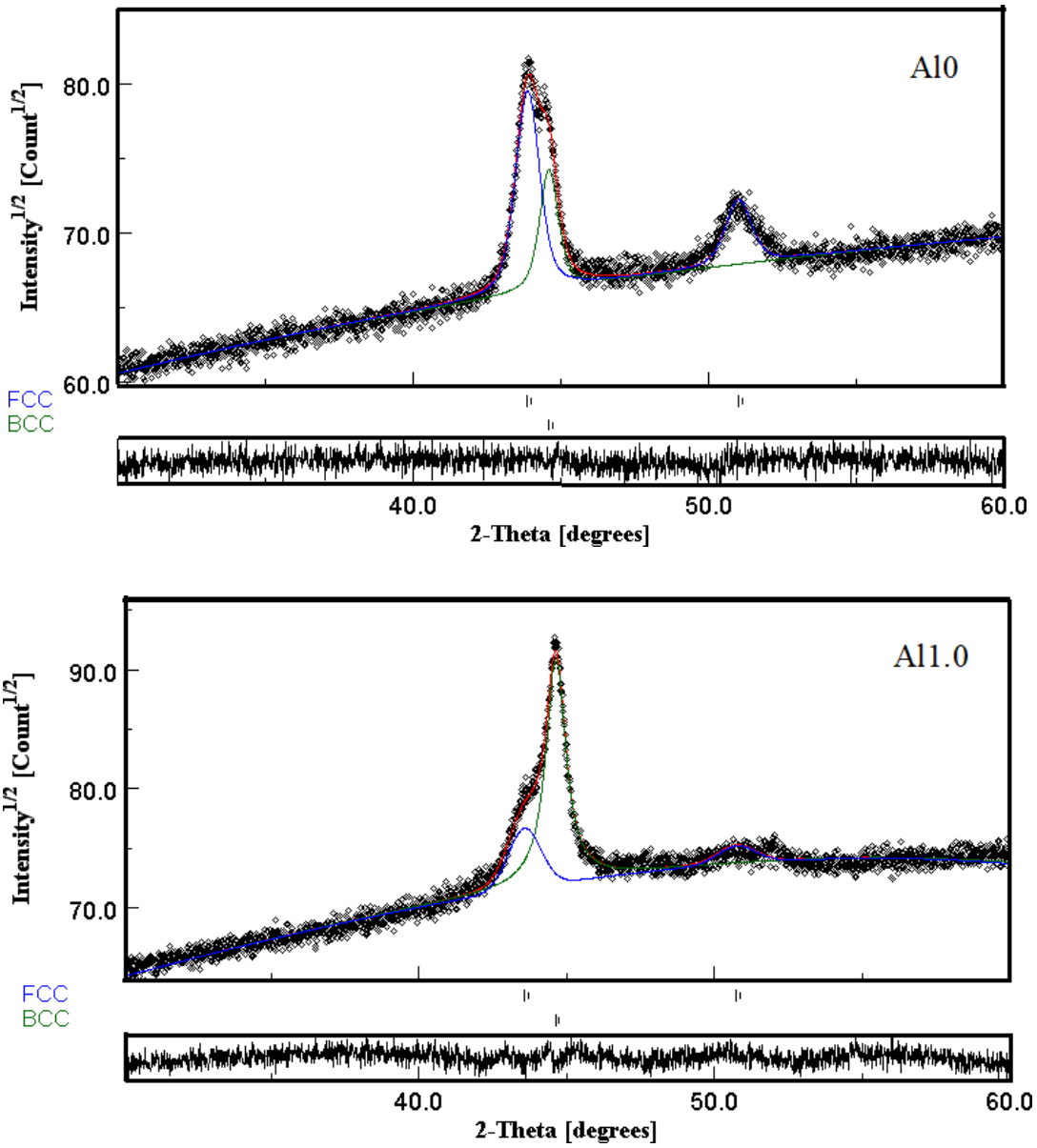


Figure III.3: *Rietveld refinement of the ball-milled Al0 and Al1.0 powders for 24 h.*

The misfit in the mixing enthalpy of the constituent elements affects the configurational entropy of a random solid solution. Moreover, the higher the magnitude of the mixing enthalpy of binaries scales, the more probable the local chemical short-range order. Hence, to obtain a random solid solution, it is important to minimize both the magnitude and fluctuation in the mixing and formation enthalpy associated with a multicomponent alloy because the enthalpy acts like “resistance” against the random solid solution formation. This disagrees with the higher configurational entropy, which favors random solid solution over other phases.

Table III.1: Characteristics of the starting Al, Cr, Fe, Co, and Ni elements: atomic radii (r), Valence Electron Concentration (VEC), melting temperature (T_m), crystal structure, activation energy (Q) [03], and enthalpies of mixing for binary pairs of the multicomponent alloy (ΔH_{mix}) [04].

Element		**Al**	**Cr**	**Fe**	**Co**	**Ni**
r (nm)		0.143	0.128	0.124	0.125	0.125
VEC		3	6	8	9	10
T_m (K)		933	2180	1811	1768	1728
Crystal structure		FCC	BCC	BCC	HCP	FCC
Q (kJ/mol)		210.4	313	309	270	304
ΔH_{mix} (kJ/mol)	**Al**	/	–10	–11	–19	–22
	Cr	–10	/	–1	–4	–7
	Fe	–11	–1	/	–1	–2
	Co	–19	–4	–1	/	0
	Mn	–22	–7	–2	0	/

Crystal structures, lattice parameters, average crystallite sizes, microstrains, and weight fractions are summarized in Table 2. The presence of BCC and FCC solid solutions in the Al0 and Al1.0 samples is different from those obtained earlier [05-07], where it has been reported that the crystal structure consists of a single FCC phase. Those discrepancies can be attributed mainly to the preparation conditions. Indeed, a single-phase FCC solid solution was obtained after 20–40 h in the mechanically alloyed CrMnFeCoNi using a planetary ball mill (RETSCH PM-400), a ball-to-powder ratio of 10:1, and a rotation speed of 400 rpm [08]. Moreover, it has been reported that the FeCoCrNiMn HEA prepared by arc melting followed by homogenization for 48 h at 1200 ◦C exhibited a single FCC structure. Furthermore, the FCC structure was stable by long-term annealing at 900 ◦C but became thermodynamically unstable at intermediate temperatures of 700 °C and 500 °C [09]. The phase's stability in HEAs can be affected by changes in composition. For example, the addition of Al to the CrMnFeCoNi alloy promotes a BCC structure over FCC one. In the composition range of 8 at% < Al < 16 at%, Al addition leads to a change from FCC to a mixture of FCC and BCC, while a single BCC phase is obtained for higher Al content [10]. Usually, the addition of a new element to a multicomponent system leads to much larger thermodynamic changes, which depend on the type of the element added. For example, CoCrFeNiAl and CoCrFeNiMn have similar configurational entropies but are

significantly different in their properties and structures, which are predominantly BCC and exclusively FCC, respectively [11]. The type of solid solution (BCC, FCC, or BCC + FCC) in the HEAs can be controlled by the valence electron concentration (VEC). Hence, a BCC solid solution can be formed with a VEC lower than 6.87, FCC with a VEC higher than 8, and a mixture of BCC + FCC with a VEC in the range of 6.87–8. It seems that the proposed criterion to predict the formation of a single FCC solid solution [11] is not valid for the Al0 powders, although the VEC is equal to 8.25. This means that the crystal structure and phase formation can be influenced by other parameters, mainly in the MA process.

Table III.2: Lattice parameter, a, crystallite size, <L>, micro strains $<\sigma^2>^{1/2}$, and weight fractions obtained from the Rietveld refinement of the XRD patterns of the ball-milled Al0 and Al1.0 HEAs for 24 h.

Sample	Structure	a ± 10^{-3} (Å)	<L> ±1 (Å)	$<\sigma^2>^{1/2}$ (%)	Fraction ±1 (wt %)
Al0	FCC	3.586	214	0.05	75.5
	BCC	2.882	239	0.03	24.5
Al1.0	FCC	3.596	341	0.4	11.7
	BCC	2.870	154	0.02	88.3

The VEC number is valuable for predicting the crystal structures of compounds. Nevertheless, these rules mean that any misfit in the physical/chemical properties of the constituent elements of an alloy is not in favor of a random solid solution. He et al. have suggested the idea of entropic stabilization [13]. The notion of entropy stabilization involves increasing disorder within a material to stabilize a specific structure. It should involve the following measures: (1) to increase the number of elements, (2) to minimize all sorts of property misfits (atomic size, chemical bond, etc.), and (3) to maximize the melting temperature. By increasing the number of constituent elements, the configurational entropy of the system increases because the material has more ways to distribute its constituent atoms, enhancing the disorder at higher temperatures. Moreover, alloying elements with different properties leads to stress/strain and induces the formation of ordered structures, which are usually less entropically favored. Thus, selecting elements with similar properties reduces the stress, enhances the disorder, and minimizes property misfits.

The lattice parameter of the BCC solid solution in the mechanically alloyed Al0 powders (a = 2.882 Å) is slightly higher than that of Al1.0 (a = 2.870 Å), and their relative deviations are about 0.59% and 0.17%, respectively. The small expansion of the crystal lattice

can be related to the slight misfit in the atomic radii of the elemental powders. Moreover, the lattice parameter of the FCC solid solution of the Al0 powders (a = 3.586 Å) is lower than that of the Al1.0 powders (a = 3.596 Å), and their relative deviations reach as much as 1.64% and 1.93%, respectively. The significant increase in the lattice parameter of the FCC solid solution for the Al1.0 powders can be related to the aluminium addition with a larger atomic radius (0.143 nm) compared to the other elements. The lattice distortion of the two solid solutions might be attributed to the severe plastic deformation that introduces many types of structural defects and an increase in their density during the milling process. Likewise, the significant lattice distortion of the FCC solid solution can be due to the nature of the starting powders, particularly the ductility of Ni and Al, and the lower fusion temperature of aluminium (660 °C).

The crystallite size of Al0 powders is almost identical for FCC and BCC solid solutions (~21–24 nm) but varies slightly for the Al1.0 alloy (34–15 nm). Moreover, the microstrains, which are more important for the FCC than BCC solid solutions, agree well with the crystal lattice distortion. The microstructure of HEAs may be affected by many factors, such as high entropy, severe lattice distortion, etc. [14]. The weight fraction of the BCC solid solution, which may include both A2 and B2 structures, increases from ~25% for Al0 to ~88% for Al1.0 alloy. Simultaneously, the weight fraction of the FCC solid solution decreases from ~75% for Al0 to ~12% for Al1.0 alloy. The increase in the weight fraction of the BCC solid solution for the Al1.0 alloy evidences the Al addition. Indeed, although aluminium has an FCC structure, it acts as a strong BCC stabilizer, and its addition enhances the strength of the alloy at the cost of reduced ductility. The increase in the BCC weight fraction with aluminium addition is in suitable agreement with the reported results earlier in the literature [11].

III.2.2. SEM analysis

Figure III.4 shows typical images of the mechanically alloyed Al0 and Al1.0 powders for 24 h. The powder particles exhibit both small and large particles with irregular shapes and sizes due to cold welding. Indeed, the existence of smaller and bigger particles is due to the competition between fracturing and cold welding during the milling process. One can emphasise that during the milling process, the dominant forces of repeated cold welding, agglomeration, deagglomeration, and fracturing inside the jars result in sized particles.

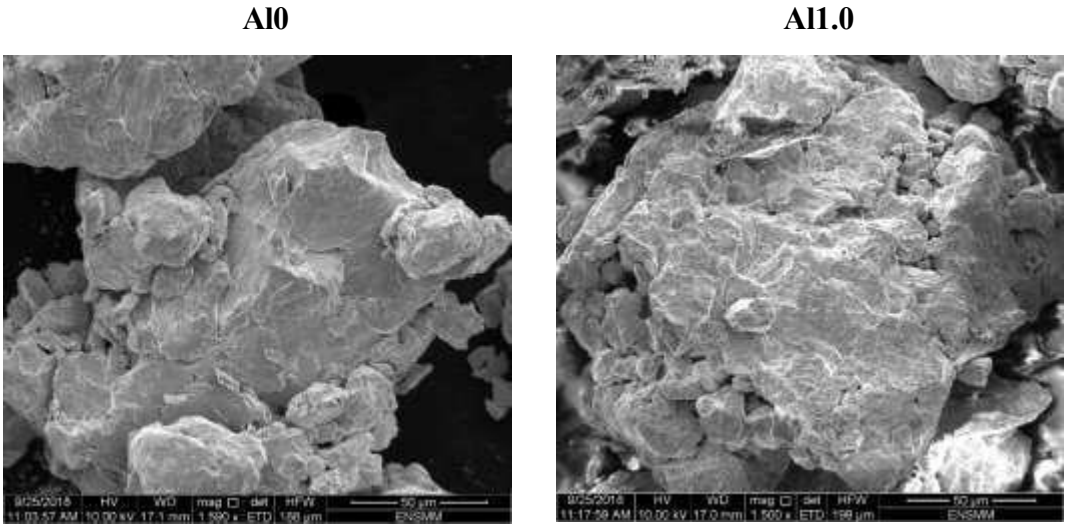


Figure III.4: *SEM photos of the ball-milled Al0 and Al1.0 powders.*

III.3. Magnetic properties

The hysteresis cycle gives information on the magnetic behavior and magnetization changes of the HEAs powders, at room temperature, as shown in Figure III.5. The hysteresis loops reveal that the samples are soft magnetic materials. The sigmoidal shape is a characteristic of ferromagnetic character. The magnetization reaches a maximum value that depends on its intrinsic properties, such as its chemical composition and crystal structure. Therefore, the reduced M_s values (M_s = 22 emu/g) of the Al0 and Al1.0 powders (Ms = 29 emu/g) can be mainly attributed to the formation of the FCC solid solutions.

The coercivity is an extrinsic property that can be affected by the microstructure (crystallite size, particle size, morphology, grain boundaries, etc.) and crystal defects such as vacancies, interstitials, and dislocations. The values of H_c (150–189 Oe) can be due to the important amount of structural defects that are induced into the powder particles during the milling process. Thus, the produced powders have semi-hard magnetic behavior. The squareness ratio M_r/M_s is a dimensionless quantity between 0 and 1 that measures how square the loop is. M_r/M_s is used to characterize how a material retains its magnetization when the external magnetic field is removed. It provides information regarding whether particles are multiple magnetic domains ($M_r/M_s < 0.1$), pseudo-single domains ($0.1 < M_r/M_s < 0.5$) or single magnetic domains ($M_r/M_s > 0.5$). According to the M_r/M_s ratio values, which are about 0.16 and 0.17 for Al0 and Al1.0, respectively, the mechanically alloyed HEAs are pseudo-single domains.

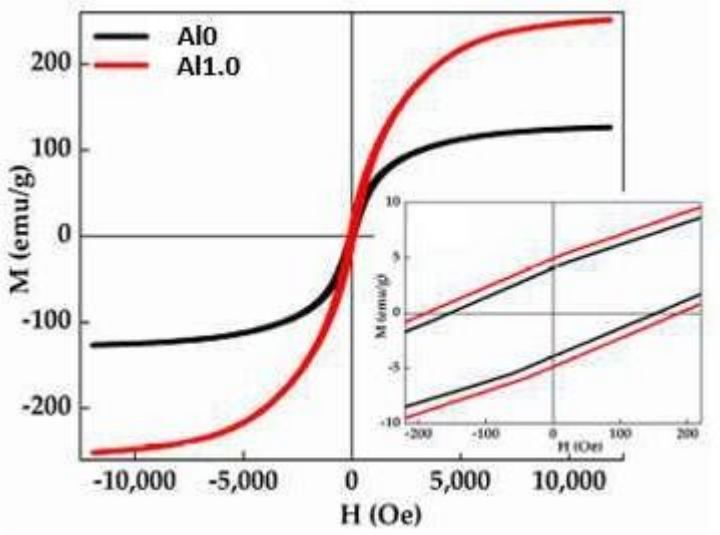


Figure III.5: *Hysteresis loops of the ball-milled Al0 and Al1.0 powders.*

1. M. Vaidya, K.G. Pradeep, B.S. Murty, G. Wilde, S.V. Divinski. Bulk tracer diffusion in CoCrFeNi and CoCrFeMnNi high entropy alloys. *Acta Mater.* (2018) 146:211–224.
2. A. Takeuchi, A. Inoue. Classification of bulk metallic glasses by atomic size difference, heat of mixing and period of constituent elements and its application to characterization of the main alloying element. *Mater. Trans.* (2005) 46: 2817–2829.
3. L. Lutterotti. MAUD Program Version 2.992 [Internet]. [Cited 2021 Nov 28]. Available from: https://maud.radiographema.com/
4. H.M. Rietveld. The Rietveld method. *Phys Scr.* (2014) 89:098002.
5. J.W. Yeh. Recent progress in high entropy alloys. *Ann. Chim. Sci. Mat.* (2006) 31:633–48.
6. N. Kumar, C.S. Tiwary, K. Biswas. Preparation of nanocrystalline high-entropy alloys via cryomilling of cast ingots. *J. Mater. Sci.* (2018) 53:13411–23.
7. Y.Y. Zhao, T.G. Nieh. Correlation between lattice distortion and friction stress in Ni-based equiatomic alloys. *Intermetallics* (2017) 86 :45–50.
8. Y. Xing, C.J. Li, Y.K. Mu, Y.D. Jia, K.K. Song, J. Tan, et al. Strengthening and deformation mechanism of high-strength CrMnFeCoNi high entropy alloy prepared by powder metallurgy. *J. Mater. Sci. Technol.* (2023) 132:119–31.
9. F. Otto, A. Dlouhý, K.G. Pradeep, M. Kuběnová, D. Raabe, G. Eggeler, et al. Decomposition of the single-phase high-entropy alloy CrMnFeCoNi after prolonged anneals at intermediate temperatures. *Acta Mater.* (2016) 112:40–52.
10. J.Y. He, W.H. Liu, H. Wang, Y. Wu, X.J. Liu, T.G. Nieh, et al. Effects of Al addition on structural evolution and tensile properties of the FeCoNiCrMn high-entropy alloy system. *Acta Mater.* (2014) 62:105–13.
11. Y. Zhang, T.T. Zuo, Z. Tang, M.C. Gao, K.A. Dahmen, P.K. Liaw, et al. Microstructures and properties of high-entropy alloys. *Prog. Mater. Sci.* (2014) 61:1–93.
12. U. Mizutani. Hume-Rothery Rules for Structurally Complex Alloy Phases. Boca Raton, FL: CRC Press; 2016.
13. Q.F. He, Y.F. Ye, Y. Yang. Formation of Random Solid Solution in Multicomponent Alloys: From Hume-Rothery Rules to Entropic Stabilization. *J. Phase Equilib. Diffus.* (2017) 38:416–25.
14. W. Guo, J. Li, M. Qi, Y. Xu, H.R. Ezatpour. Effects of heat treatment on the microstructure, mechanical properties and corrosion resistance of AlCoCrFeNiTi0.5 high-entropy alloy. *J. Alloys Compd.* (2021) 884:161026.

General Conclusion

The effect of aluminium addition on the structure, microstructure, morphology, and magnetic properties of the synthesized $CoCrFeNiAl_x$ (x = 0, and 1 mol, named as Al0, and Al1.0, respectively) high-entropy alloys has been studied. The powders were elaborated using the mechanical alloying process. The characterization techniques are X-ray diffraction (XRD), Scanning electron microscopy (SEM), and vibrating sample magnetometer (VSM). The Rietveld refinement of the XRD patterns reveals the formation of two disordered solid solutions. The aluminium addition causes a slight change in the lattice parameter ($a_{(FCC)}$ is in the range of 8.38−9.4 nm and $a_{(BCC)}$ varied between 8.38−9.4 nm). The crystallite size values are in the range of 15–34 nm. Morphology micrographs are investigated with SEM technique; it showed irregular size of the particles. Furthermore, the mechanically alloyed powders exhibit typical hysteresis loops of ferromagnetic materials. The addition of Al affects the saturation magnetization and coercivity. The saturation magnetization, coercivity, and squareness 9atio Mr/Ms values are in the range of 22–29 emu/g, 150–189 Oe, and 0.16–0.17, respectively. Both the produced powders fall into pseudo-single domain. As perspective, it would be interesting to optimize the elaboration conditions and study the mechanic and corrosive properties.